

deviation of the observed structure factor ($|F_o|$) due to counting statistics. Scattering factors were taken from *International Tables for X-ray Crystallography*.²¹

In view of the rather high R value obtained and the anisotropy of some of the thermal ellipsoids, indicating disorder or inaccuracy of the data due to loss of nitromethane, we have decided to perform a low-temperature structure determination, the results of which will be published elsewhere.

Determination of the Association Constants. All ¹H NMR spectra were recorded on a Bruker 80-MHz apparatus with a B-VT-1000 temperature accessor. All measurements were carried out in deuteriobenzene with Me₄Si as the internal standard. Considering only 1:1 complexation (model I), the association constant can be expressed by eq 3 in which

$$K = \frac{[\text{CE}\cdot\text{M}]}{([\text{CE}]_0 - [\text{CE}\cdot\text{M}])([\text{M}]_0 - [\text{CE}\cdot\text{M}])} \quad (3)$$

$[\text{CE}]_0$ and $[\text{M}]_0$ are the initial concentrations of respectively crown ether and uncharged molecules. The observed chemical shift of the protons of the uncharged guest molecules is given by eq 4, in which δ_M is the

$$\delta_{\text{obsd}} = \chi_M \delta_M + \chi_{\text{CE}\cdot\text{M}} \delta_{\text{CE}\cdot\text{M}} \quad (4)$$

chemical shift of the uncharged molecule, $\delta_{\text{CE}\cdot\text{M}}$ is the chemical shift of this molecule in the complex, $\chi_M = ([\text{M}]_0 - [\text{CE}\cdot\text{M}])/[\text{M}]_0$, and $\chi_{\text{CE}\cdot\text{M}} = [\text{CE}\cdot\text{M}]/[\text{M}]_0$. For a series of samples in which both CE and M concentrations were varied, the chemical shift was measured, and in an iterative procedure a minimum is found by eq 5. By varying K and

$$F = \sum_i (\delta_{\text{obsd}_i} - \chi_M \delta_M - \chi_{\text{CE}\cdot\text{M}} \delta_{\text{CE}\cdot\text{M}})^2 \quad (5)$$

$\delta_{\text{CE}\cdot\text{M}}$, both χ_M and $\chi_{\text{CE}\cdot\text{M}}$ are calculated from eq 6. If one takes into $[\text{CE}\cdot\text{M}] = \frac{1}{2}([\text{CE}]_0 + [\text{M}]_0 + 1/K) - [([\text{CE}]_0 + [\text{M}]_0 + 1/K)^2 - 4[\text{CE}]_0[\text{M}]_0]^{1/2}$ (6)

account that for the minimum $\partial F/\partial \delta_{\text{CE}\cdot\text{M}}$ must be zero, then $\delta_{\text{CE}\cdot\text{M}}$ can be expressed according to

$$\delta_{\text{CE}\cdot\text{M}} = (\sum_i \delta_{\text{obsd}_i} \chi_{\text{CE}\cdot\text{M}_i} - \sum_i \chi_{\text{CE}\cdot\text{M}_i} \chi_M \delta_M) / \sum_i \chi_{\text{CE}\cdot\text{M}_i}^2 \quad (7)$$

By substitution of eq 7 into eq 5, F needs only to be minimized for K .

When both 1:1 and 1:2 complexation (model II) takes place, the equations can be easily modified. In this model we have assumed that the chemical shifts of the uncharged molecule in the 1:1 and 1:2 complex are the same.²² The modified function F has to be minimized now for $K^{1:1}$, $K^{1:2}$, and $\delta_{\text{CE}\cdot\text{M}}$.

The chemical shifts of uncharged molecules in benzene depend on concentration and temperature. There is a linear relation between concentration and chemical shift at a certain temperature. The chemical shifts of the free uncharged molecules at different temperatures were corrected by using that linear relation. For a series of measurements, the data were fitted for both 1:1 complexation (model I) and 1:1 and 1:2 complexation (model II). The best model was the one in which the calculated data agree with the experimental data.

Registry No. 1 (CH₃NO₂), 82064-74-2; 1 (CH₃NO₂)₂, 55075-34-8; 1 (CH₃CN), 60336-83-6; 1 (CH₃CN)₂, 55075-35-9; 1 [CH₂(CN)₂], 63726-93-2; 1 [CH₂(CN)₂]₂, 61994-85-2; 2 (CH₃NO₂), 82064-75-3.

Supplementary Material Available: Tables of atomic thermal parameters and a list of observed and calculated structure factors (10 pages). Ordering information is given on any current masthead page.

(22) In the case of nitromethane, calculations were also carried out in which the chemical shift of the 1:1 complex was taken different from that of the 1:2 complex. Both types of calculations give the same results (within experimental error).

Dithizone Adsorption at Metal Electrodes. 4. Voltammetric and Surface Raman Spectroelectrochemical Investigation at a Copper Electrode

Jeanne E. Pemberton[†] and Richard P. Buck*

Contribution from the Kenan Laboratories of Chemistry, University of North Carolina, Chapel Hill, North Carolina 27514. Received September 8, 1981

Abstract: Cyclic voltammetric and surface Raman spectroelectrochemical behavior of the anion of dithizone (diphenylthiocarbazone), HDz⁻, has been characterized at a Cu electrode in aqueous alkaline media. The cyclic voltammetry suggests very strong interaction of HDz⁻ with the Cu surface. In the presence of HDz⁻, significant oxidation of the Cu surface does not take place until potentials greater than 0.2–0.3 V are reached. The surface Raman spectroelectrochemical data are consistent with strong adsorption of HDz⁻ at the Cu surface at potentials negative of the oxidation potential. Very little control of surface HDz⁻ population can be realized through alteration of the potential. This is in contrast to the previous behavior observed at Ag. The surface species observed at potentials more positive than the oxidation potential of HDz⁻ is the disulfide. The effect of solubility on the extent of adsorption was also investigated. The surface Raman data indicate that adsorption of HDz⁻ in pH 10 solution is significantly greater than that in pH 12 solution in which HDz⁻ is more soluble. On the basis of the similarity of the surface spectra obtained and the spectrum of copper(II) dithizonate, an approximate orientation of HDz⁻ at the Cu/solution interface is proposed.

The utility of Raman spectroscopy as a probe of molecules at or near electrode surfaces has been amply demonstrated in the recent literature.^{1,2} The sensitivity constraints imposed by the normal Raman scattering process for surface species can be overcome by exploitation of surface-enhanced Raman scattering (SERS), resonance Raman scattering (RRS), or a combination

of these two phenomena (SERS + RRS) to enhance the Raman intensities to a readily measured level. The use of SERS requires the proper choice of both metal substrate and excitation frequency. SERS has been verified only at Ag,¹ Cu, and Au^{3–6} metal surfaces,

(1) Van Duyne, R. P. In "Chemical and Biochemical Applications of Lasers", Moore, C. B., Ed.; Academic Press: New York, 1979; Vol. 4, pp 101.

(2) Furtak, T. E.; Reyes, J. *Surf. Sci.* 1980, 93, 351.

(3) Wenning, U.; Pettinger, B.; Wetzel, H. *Chem. Phys. Lett.* 1980, 70, 49.

[†] Present address: Department of Chemistry, University of Arizona, Tucson, Arizona 85721

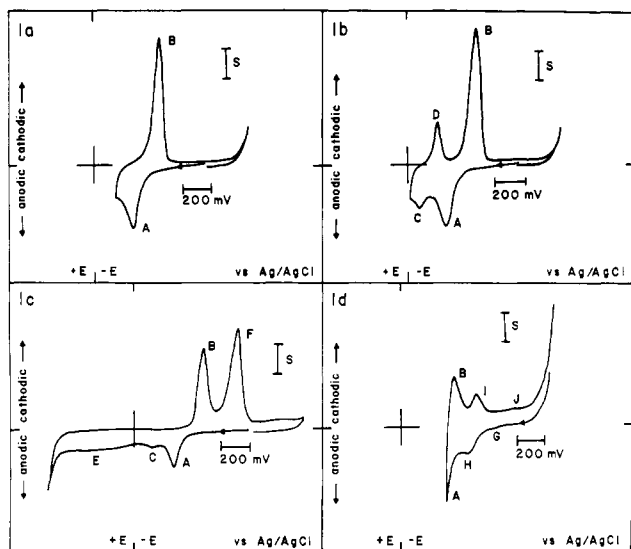
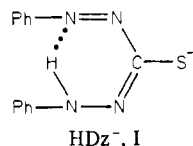


Figure 1. Cyclic voltammetry of Cu in pH 12 aqueous alkaline buffer solution: (a) $\nu = 100$ mV/s, $S = 100$ μ A; (b) $\nu = 100$ mV/s, $S = 100$ μ A; (c) $\nu = 100$ mV/s, $S = 100$ μ A; (d) $\nu = 500$ mV/s, $S = 111$ μ A. Processes A through J are discussed in the text.

and the possibility of SERS at Hg^7 and Ni^8 has been noted. The excitation frequency is also a critical variable in the SERS mechanism. The greatest enhancement at Ag is observed with blue-green excitation¹, while excitation must be in the red for SERS to be observed at Cu and Au.³⁻⁶

The use of RRS requires that the excitation frequency is within an electronic transition of the molecule of interest. When the energy region of the electronic transition for an adsorbate at a SERS metal is coincident with the SERS-allowed frequency region of the metal, both types of intensity enhancement can be realized simultaneously. This combined process has been termed SERS + RRS by Van Duyne.⁹

In previous surface Raman spectroelectrochemical studies of dithizone anion (HDz^- , I) adsorbed at a Ag electrode,^{10,11} the



combined SERS + RRS enhancement was realized with 488.0-nm excitation. In an attempt to determine differences in the interaction of HDz^- with various metal-electrode surfaces, these studies were extended and a series of experiments were performed at a Cu electrode. All of these studies were carried out with 488.0-nm excitation. On the basis of results in the recent literature on SERS at Cu surfaces,³⁻⁶ this excitation frequency should yield spectra that are only resonance enhanced. This report details voltammetric and surface Raman spectroelectrochemical investigations of HDz^- adsorption at a Cu electrode in aqueous alkaline solution.

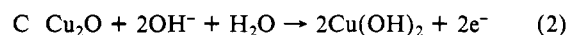
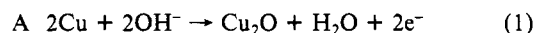
Results and Discussion

Cyclic Voltammetry of HDz^- at Cu in Alkaline Media. Figure 1 shows the cyclic voltammograms obtained from a freshly polished Cu electrode immersed in a pH 12 aqueous buffer solution. These voltammograms are similar to numerous other cyclic voltammetric

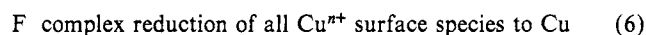
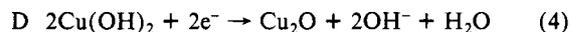
investigations of Cu in alkaline media that have been previously reported.¹²⁻¹⁶ The voltammograms in Figures 1a-c illustrate the effect of anodic potential scan limit on the resulting voltammogram. In Figure 1a, the scan was reversed at ca. -0.15 V. In this potential region, oxidation process A and reduction process B are observed. When the potential is taken further anodic to 0.0 V, a second oxidation process (C) and corresponding reduction process (D) are observed (Figure 1b). Figure 1c shows the voltammogram obtained when the potential is scanned anodically to solvent breakdown (ca. 0.60 V). A third oxidation process (E) is observed. On the reverse scan, reduction process D is no longer observed. Reduction process B is still present, and a new reduction process (F) becomes quite prominent. All of the redox processes observed in Figures 1a-c can be attributed to the formation and removal of Cu surface species. On the basis of the earlier work of Ambrose et al.¹² and others on Cu in alkaline media,¹³⁻¹⁶ Scheme I is proposed to account for these surface processes.

Scheme I

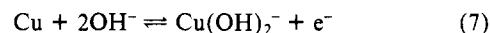
Forward Scan



Reverse Scan



A closer examination of the potential region preceding (i.e., more negative than) process A reveals the presence of other redox processes. Figure 1d shows this potential region in greater detail. In addition to process A, two smaller oxidation waves, G and H, are observed. The corresponding reduction processes are labeled I and J. A recent cyclic voltammetric and ellipsometric investigation of these processes on Cu has been reported by Droog et al.¹⁶ They concluded that the oxidation processes represent electroadsorption of oxygen species and that the reduction processes represent the corresponding desorption processes. These authors do not describe the oxygen species that is adsorbed in this potential region. However, they do report that this electroadsorption process occurs in two successive stages, each represented by a peak corresponding to a different submonolayer state with a different adsorption energy. Ambrose et al.¹² assigned a similar set of waves to adsorption and desorption of hydroxyl species according to



This process is assumed to be occurring in our system. It is possible that the two observed waves arise from adsorption of hydroxyl species according to eq 7 on different crystal faces of Cu and, therefore, occur at different energies.

Figure 2 shows the cyclic voltammetry observed at a freshly polished Cu electrode in pH 12 buffer solution in the presence of 10^{-3} M HDz^- . The redox behavior at Cu is dominated by the presence of the reducible azo functionality and the oxidizable sulfhydryl functionality.¹⁷ The observed redox behavior of HDz^- at Cu is similar to that at Ag, although some important differences exist. A detailed analysis of the redox behavior of HDz^- at Ag

(4) Pettinger, B.; Wenning, U.; Wetzell, H. *Surf. Sci.* **1980**, *101*, 409.

(5) Allen, C. S.; Schatz, G. C.; Van Duyne, R. P. *Chem. Phys. Lett.* **1980**, *75*, 201.

(6) Marinyuk, V. V.; Lazorenko-Manevich, R. M.; Kolotyrykin, Y. M. *J. Electroanal. Chem.* **1980**, *110*, 111.

(7) Naaman, R.; Buelow, S. J.; Cheshnovsky, O.; Herschbach, D. R. *J. Phys. Chem.* **1980**, *84*, 2692.

(8) Yamada, H.; Yamamoto, Y. *Chem. Phys. Lett.* **1981**, *77*, 520.

(9) Cotton, T. M.; Schultz, S. G.; Van Duyne, R. P. *J. Am. Chem. Soc.* **1980**, *102*, 7960.

(10) Pemberton, J. E.; Buck, R. P. *J. Phys. Chem.* **1981**, *85*, 248.

(11) Pemberton, J. E.; Buck, R. P. *Anal. Chem.* **1981**, *53*, 2263.

(12) Ambrose, J.; Barradas, R. G.; Shoesmith, D. W. *J. Electroanal. Chem.* **1973**, *47*, 47.

(13) Macdonald, D. D. *J. Electrochem. Soc.* **1974**, *121*, 651.

(14) Fletcher, S.; Barradas, R. G.; Porter, J. D. *J. Electrochem. Soc.* **1978**, *125*, 1960.

(15) Luna de Medina, A. M. C.; Marchiano, S. L.; Arvia, A. J. *J. Appl. Electrochem.* **1978**, *8*, 121.

(16) Droog, J. M.; Alderliesten, C. A.; Alderliesten, P. T.; Bootsma, G. A. *J. Electroanal. Chem.* **1980**, *111*, 61.

(17) Tomcsanyi, L. *Anal. Chim. Acta* **1974**, *70*, 411.

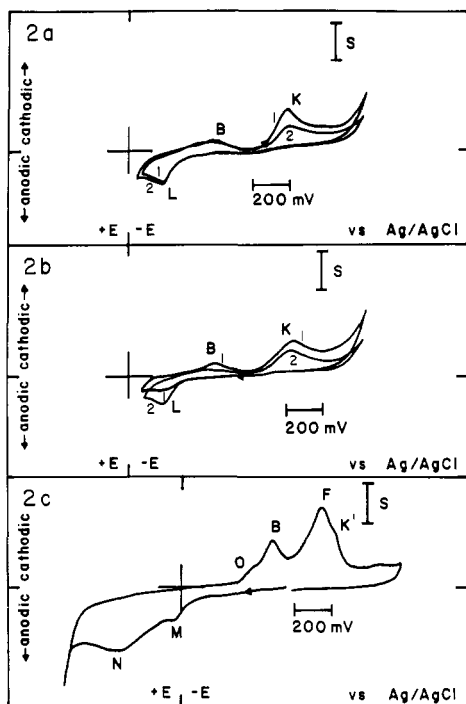
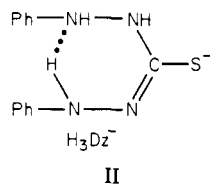


Figure 2. Cyclic voltammetry of 10^{-3} M HDz⁻ in pH 12 buffer solution at a Cu electrode: (a) $\nu = 100$ mV/s, $S = 100$ μ A; (b) $\nu = 100$ mV/s, $S = 100$ μ A; (c) $\nu = 100$ mV/s, $S = 100$ μ A. Processes B through O are discussed in the text.

has been previously reported from this laboratory.¹⁸

Figure 2, a and b, shows the voltammograms obtained from a Cu electrode when scanning initially toward more negative and more positive potentials from the initial potential, respectively. Reduction process K is observed in both instances at ca. -0.80 V. This wave represents reduction of HDz⁻ at the azo group to the corresponding H₃Dz⁻ hydrazo species, diphenylthiocarbazide (II).¹⁷⁻¹⁹ The peak current measured for this wave is significantly



smaller than would be predicted by voltammetric theory. Also notable for this reduction process at Cu is the absence of the preceding wave that was observed in the voltammograms obtained with a Ag working electrode.¹⁸ The wave measured at more negative potentials at Ag, ca. -0.78 V, was attributed to reduction of surface HDz⁻ species, and the preceding wave was attributed to reduction of solution HDz⁻ species. These assignments were made on the basis of cyclic voltammetric, surface Raman spectroscopic, and XPS results. They show weak or no adsorption of H₃Dz⁻ at the Ag surface and indicate that an analysis of the data in terms of a prewave for adsorption of the redox product is inappropriate.¹⁸

The peak current and peak potential data measured in this study at Cu suggest that process K represents reduction of only surface-adsorbed HDz⁻ to the corresponding H₃Dz⁻. The shape and peak current of this wave indicate that this reduction is irreversible. Furthermore, from the absence of the preceding wave, it seems reasonable to conclude that electron transfer through the surface HDz⁻ species to solution HDz⁻ species either does not occur or occurs at a greatly reduced heterogeneous electron-transfer rate relative to the time scale of the cyclic voltammetric experiment. Retardation of electron transfer could occur by electrostatic re-

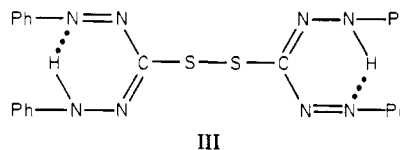
pulsion of the solution HDz⁻ by the anionic HDz⁻ adsorbate in a manner analogous to that observed previously by Lane and Hubbard for charged adsorbates and solubilized redox species at a Pt working electrode.²⁰ If this were the case, however, one would expect that the same behavior would be observed at Ag. As indicated above, reduction of solution HDz⁻ is apparent at Ag and speaks against this electrostatic repulsion argument for the HDz⁻ system at Cu.

An alternative explanation, and one that is more easily corroborated by the collective data at Ag and Cu, is that electron transfer through surface HDz⁻ species to solution species cannot occur. While such restricted electron transfer through adsorbates to solution species is not general for all adsorbates, it has been noted previously for many systems, and has been commonly known as electrode fouling. If the interaction of HDz⁻ with the Cu surface is stronger than with the Ag surface (i.e., one complete monolayer of HDz⁻ is formed at Cu), then electron transfer with solution HDz⁻ species will not occur. If at Ag, the interaction is weaker (i.e., less than a complete monolayer is formed), "bare" patches of the Ag metal will exist through which electron transfer can take place. This explanation of greater interaction of HDz⁻ with Cu than with Ag is further substantiated by the surface Raman data discussed below.

Voltammograms in Figure 2a,b show that oxidation process L, which occurs at ca. -0.175 V, is coupled to reduction process K. The peak separation between waves K and L is large, and is also observed at Ag. In that case, the peak separation was attributed to greater adsorption of the azo form (HDz⁻) than that of the hydrazo form (H₃Dz⁻) and to inhibition of electrooxidation of the hydrazo form by the adsorbed HDz⁻.¹⁸

One other notable feature of the voltammograms 2a and 2b is the very small currents observed in the potential region of processes A and B. The presence of HDz⁻ in solution greatly reduces the extent of oxidation and subsequent reduction of the Cu electrode surface. These data further suggest strong interaction of HDz⁻ with the Cu surface.

Figure 2c is a voltammogram obtained when scanning to positive potentials as far as oxygen evolution at the Cu working electrode in the presence of 10^{-3} M HDz⁻. As noted in Figure 2b, very little oxidation of the Cu electrode surface occurs in the expected potential region of process A in Figure 1. The first oxidation process to be observed occurs at ca. 0.0 V (labeled as M) and represents oxidation of HDz⁻ to the corresponding disulfide compound, bis(1,5-diphenylformazan-3-yl) disulfide (III).¹⁷⁻¹⁹



Due to the insolubility of this disulfide in aqueous media, multilayers probably form on the Cu surface. As the potential is made more positive, surface oxidation begins to occur in competition with disulfide formation and adsorption. This surface oxidation results in a relatively broad wave (labeled as N) centered at ca. 0.30 V.

The Cu oxidation process is probably complex in the presence of HDz⁻ and may involve formation of partially soluble surface oxides and surface complexes of HDz⁻ and the disulfide. On the reverse scan, reduction processes B and F are observed as were observed in the absence of HDz⁻ (Figure 1). However, a prewave O on wave B and postwave K' on wave F are also observed. The prewave O probably represents reduction of any surface Cu⁺⁺ complexes that form with HDz⁻ or the disulfide oxidation product on the forward scan. These reductions would be expected to require less energy than reduction of the surface oxides. Hence, the wave is observed at potentials less negative than the oxide reduction process B. The postwave K' can most likely be attributed to reduction of solution HDz⁻ on a Cu surface newly reformed

(18) Pemberton, J. E.; Buck, R. P. *J. Electroanal. Chem.* **1982**, *132*, 291.

(19) Tomcsanyi, L. *Anal. Chim. Acta* **1977**, *88*, 371.

(20) Lane, R. F.; Hubbard, A. T. *J. Phys. Chem.* **1973**, *77*, 411.

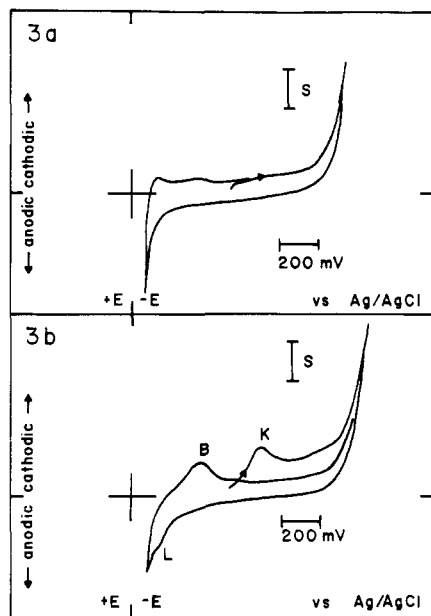


Figure 3. (a) Cyclic voltammetry of a fresh Cu electrode in 0.1 M KCl; $\nu = 100$ mV/s, $S = 22 \mu\text{A}$. (b) Cyclic voltammetry of adsorbed HDz⁻ at a Cu electrode in 0.1 M KCl; $\nu = 100$ mV/s, $S = 22 \mu\text{A}$. Adsorption conditions are discussed in the text.

Table I. Raman Spectral Bands for Cu(HDz)₂^a

frequency, ^b cm ⁻¹	rel intensity ^c	frequency, cm ⁻¹	rel intensity
724	w	1265	w
744	m	1300	s
802	m	1338	s
993	w	1390	vs
1151	s	1457	m
1165	w	1503	m
1201	s	1585	s

^a Obtained as solid powder. ^b Relative to the 488.0-nm argon ion laser excitation line. Measurement uncertainty (standard deviation) = ± 3 cm⁻¹. ^c vw = very weak, w = weak, m = medium, s = strong, vs = very strong.

from oxide reduction process F. The rate of adsorption of HDz⁻ on metal surfaces has been shown to be quite slow, even under conditions of forced convection.²¹ Hence, on the time scale of the reverse voltammetric scan, in this case of Cu, HDz⁻ adsorption has probably not occurred. Therefore, solution HDz⁻ reduction (K') occurs at a less negative potential (ca. -0.76 V) than process K for surface HDz⁻ reduction.

For independent verification of HDz⁻ adsorption at a Cu electrode, a freshly polished Cu electrode was potentiostated at -0.40 V for 10 min in 10⁻³ M HDz⁻/pH 12 solution, removed under potentiostatic control, rinsed with copious amounts of distilled deaerated water, and immersed under potential control at -0.6 V into a 0.1 M KCl solution, and a cyclic voltammogram was obtained. The results of this experiment are shown in Figure 3 along with the background voltammogram for Cu in 0.1 M KCl. As shown in Figure 3b, reduction of surface HDz⁻ occurs at ca. -0.66 V on the first scan. The variation in peak potentials is a result of the differences in pH of the test solutions used for this proton-dependent process. The coupled oxidation process is observed as a shoulder at ca. -0.13 V on the Cu oxidation process on the return scan. The surface HDz⁻ is totally reduced on the first scan, and no further reduction current is observed on the second scan.

Surface Raman Spectroelectrochemistry of HDz⁻ at Cu in Alkaline Media. pH 12 Behavior. Figure 4b shows the surface Raman spectrum obtained at a freshly polished Cu working

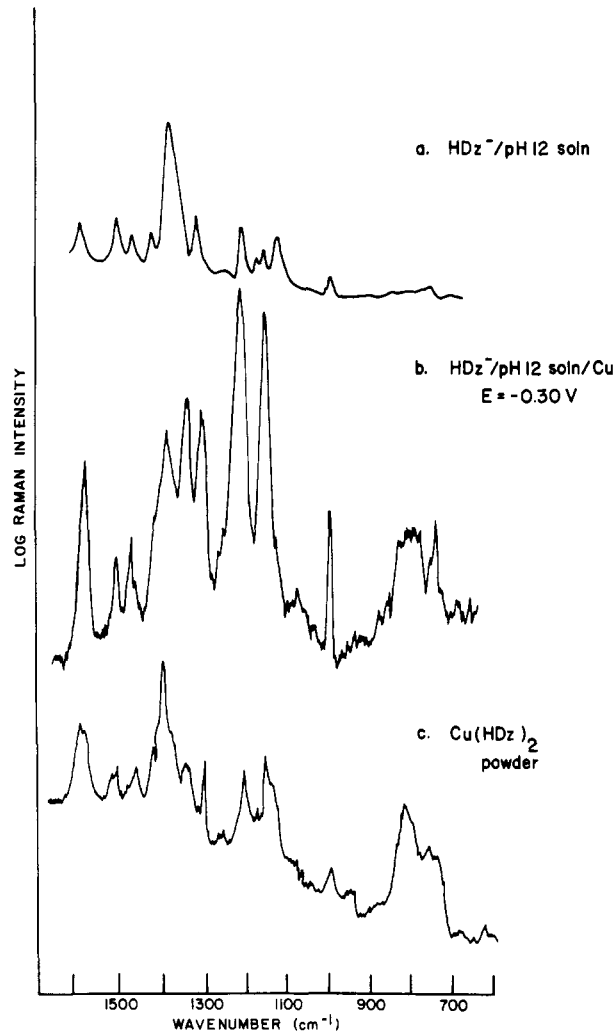


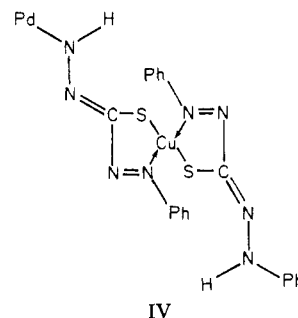
Figure 4. (a) Resonance Raman spectrum of 10⁻³ M HDz⁻/pH 12 buffer solution. (b) Surface Raman spectrum of HDz⁻ adsorbed at Cu at -0.30 V from 10⁻⁴ M HDz⁻/pH 12 solution. (c) Solid-state (powder) Raman spectrum of Cu(HDz)₂. Raman acquisition parameters are given in the text.

Table II. UV-Vis Absorption Spectrum for Cu(HDz)₂^a

λ_{max} , nm	ϵ , 10 ⁻³ cm ² mol ⁻¹	λ_{min} , nm	ϵ , 10 ⁻³ cm ² mol ⁻¹
280	25	350	15
550	45		

^a Obtained by using Cu(HDz)₂ in chloroform.

electrode potentiostated at -0.30 V in a 10⁻⁴ M HDz⁻/pH 12 solution. Shown along with this spectrum for comparison are the solution spectrum of HDz⁻ in pH 12 buffer and the solid-state spectrum of an authentic sample of Cu(HDz)₂ (IV), as Figure



4, a and c, respectively. The vibrational bands observed for solution HDz⁻ were tabulated and assigned in part 2 of this series.¹⁰ The

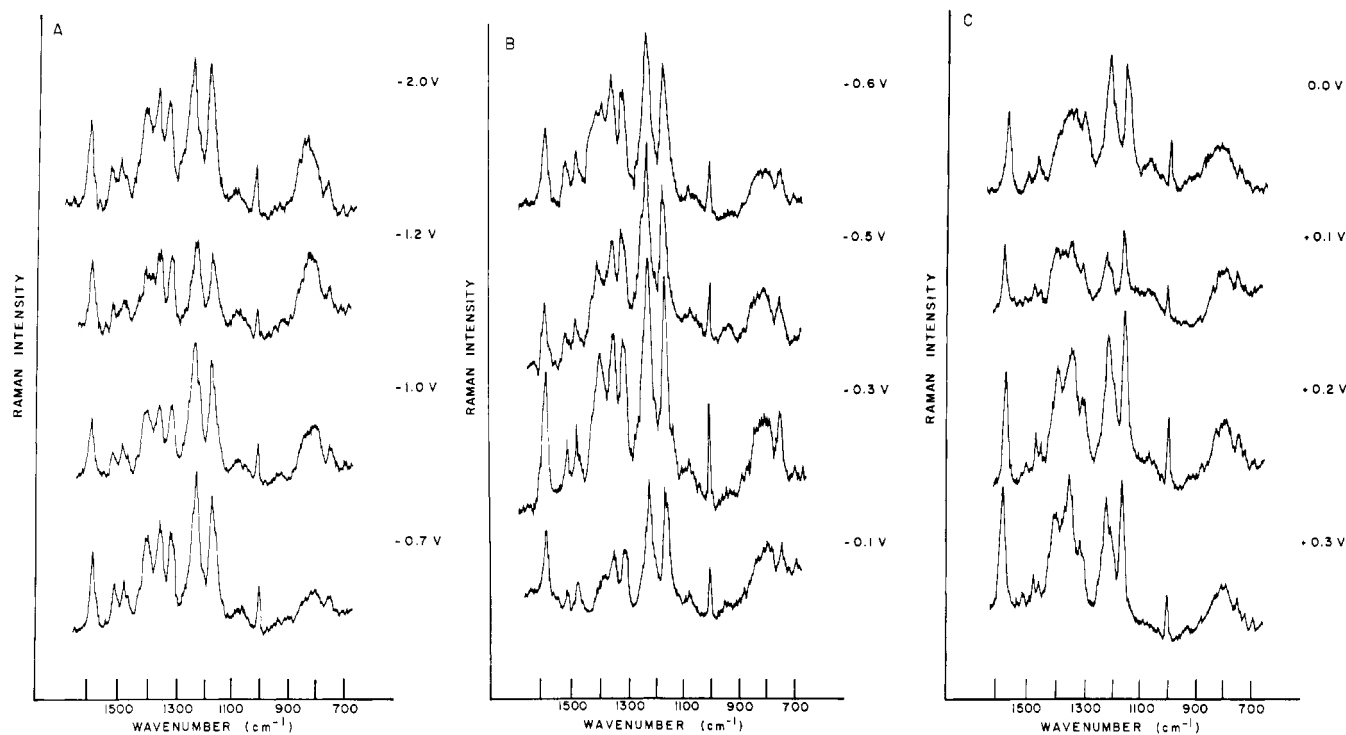


Figure 5. Surface Raman spectroelectrochemical data for 10^{-4} M HDz⁻/pH 12 solution at a Cu electrode. (A) $E_{app} = -2.0, -1.2, -1.0, -0.7$ V. (B) $E_{app} = -0.6, -0.5, -0.3, -0.1$ V. (C) $E_{app} = 0.0, 0.1, 0.2, 0.3$ V. Raman acquisition parameters are given in text.

vibrational bands and UV-vis absorption data for Cu(HDz)₂ are tabulated in Tables I and II, respectively.

All of the spectra reported in this paper were acquired in the limited frequency range between 700 and 1650 cm^{-1} . Spectra could not be acquired much above 1800 cm^{-1} as a result of very strong fluorescence. Low-frequency data (<700 cm^{-1}) could not be acquired due to very strong Raman scattering from the spectroelectrochemical cell window, which is separated from the Cu surface by only a very thin layer of solution. This interference from the cell window has been discussed in greater detail previously.²²

Comparison of spectra 4a and 4b indicates that significant structural changes take place in HDz⁻ upon interaction with the Cu surface. Further comparison of the spectra in Figure 4 suggests that evident changes in the Raman spectra between the solution HDz⁻ and the surface HDz⁻ are similar to, but not identical with, changes that are observed between solution HDz⁻ and the copper-complexed HDz⁻, Cu(HDz)₂. The series of four bands observed in the solution HDz⁻ spectrum between 1050 and 1200 cm^{-1} collapse into two major bands in both the surface HDz⁻ spectrum and the Cu(HDz)₂ spectrum. However, while these bands are only of medium intensity in the solution HDz⁻ and Cu(HDz)₂ spectra, they are very strong in intensity in the surface HDz⁻ spectrum. The band at 1369 cm^{-1} in the solution HDz⁻ spectrum, which has been assigned to the $\nu_{sym}(\text{N}=\text{C}-\text{N})$ stretch, is split into two bands in both the surface HDz⁻ and Cu(HDz)₂ spectra, one at lower frequency and one at higher frequency. However, the relative intensities of these bands are different in the surface and Cu(HDz)₂ spectra.

Potential dependence of the surface Raman behavior was then investigated. These results are shown in Figure 5 for selected potential values of Cu in a 10^{-4} M HDz⁻/pH 12 solution, and the bands are tabulated in Table III. Corresponding examples of the Cu/pH 12 solution background surface spectra are shown in Figure 6. All of the spectra presented in Figures 5 and 6 were acquired at a freshly polished Cu surface potentiostated at the correct potential. At potentials more negative than 0.0 V, very few changes are noted in the surface spectra. The peak intensities and peak positions remain relatively constant within this potential

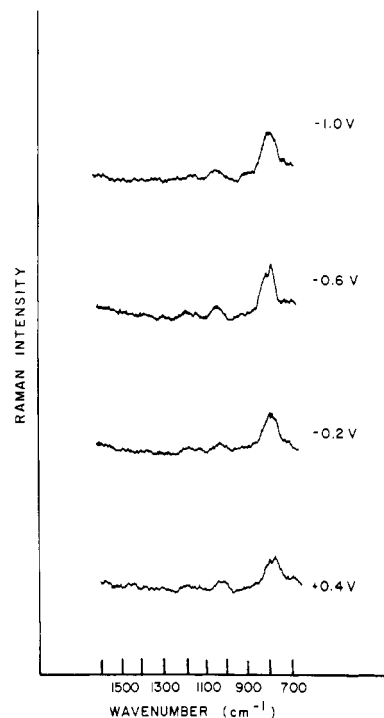


Figure 6. Surface Raman spectroelectrochemical data for Cu electrode in pH 12 buffer solution. $E_{app} = -1.0, -0.6, -0.2, 0.4$ V. Raman acquisition parameters are given in the text.

region. This behavior contrasts with that which was observed at Ag. In that case, the overall surface intensity decreased to a nondetectable level as the potential was made more negative than the potential of zero charge, and the HDz⁻ was driven off the surface by electrostatic repulsion.¹⁰ In this case at Cu, strong surface signals were measured even at potentials as far negative as -2.0 V. This is quite negative on the rational potential scale (i.e., relative to the potential of zero charge, which is estimated to be between -0.6 and -0.8 V). The presence of surface species at these negative potentials suggests a large negative free energy

Table III. Surface Raman Spectra of HDz⁻ Adsorbed Forms at Cu in pH 12 as a Function of Electrode Potential

frequency, ^a cm ⁻¹ (rel intensity) ^b		-2.00 V	-1.20 V	-1.00 V	-0.70 V	-0.60 V	-0.50 V	-0.30 V	-0.10 V	0.00 V	0.10 V	0.20 V	0.30 V
		686 (vw)	681 (vw)	684 (vw)		694 (w)		693 (w)	691 (w)	691 (w)	689 (vw)	691 (w)	691 (w)
		737 (m)	746 (w)	736 (w)	735 (vw)	740 (m)	741 (m)	747 (w)	742 (m)	751 (w)	749 (m)	729 (w)	719 (w)
		995 (m)	1004 (w)	991 (w)	994 (w)	995 (m)	993 (m)	999 (m)	998 (m)	997 (m)	998 (m)	743 (w)	747 (w)
		1155 (vs)	1159 (s)	1155 (vs)	1155 (vs)	1156 (s)	1152 (vs)	1157 (vs)	1158 (vs)	1155 (vs)	1157 (vs)	999 (m)	1000 (m)
		1213 (vs)	1210 (s)	1213 (vs)	1214 (vs)	1213 (s)	1213 (vs)	1218 (vs)	1213 (vs)	1212 (vs)	1215 (vs)	1158 (vs)	1159 (vs)
		1301 (s)	1300 (s)	1300 (s)	1302 (s)	1297 (s)	1305 (s)	1309 (s)	1308 (s)	1304 (s)	1304 (s)	1218 (vs)	1216 (vs)
		1339 (s)	1339 (s)	1340 (s)	1343 (s)	1340 (s)	1338 (s)	1341 (s)	1338 (s)	1337 (s)	1341 (s)	1309 (m)	1310 (m)
		1382 (s)	1392 (s)	1384 (s)	1386 (s)	1384 (m)	1390 (s)	1390 (s)		1355 (s)	1369 (s)		1351 (vs)
		1454 (sh)	1459 (w)	1455 (sh)						1395 (m)	1390 (s)	1351 (s)	1396 (s)
		1459 (m)	1468 (w)	1473 (w)	1470 (m)	1471 (w)	1466 (m)	1475 (m)	1471 (m)	1469 (m)	1474 (w)	1399 (s)	1457 (w)
		1505 (m)	1508 (w)	1506 (w)	1505 (m)	1504 (w)	1503 (m)	1509 (m)		1504 (w)	1474 (w)	1454 (w)	1478 (w)
		1580 (s)	1580 (s)	1581 (m)	1582 (s)	1584 (m)	1576 (s)	1582 (s)	1580 (s)	1578 (s)	1581 (s)	1511 (w)	1518 (vw)
											1581 (s)	1583 (s)	1585 (s)

^a Relative to the 488.0-nm argon ion laser excitation line. Measurement uncertainty (standard deviation) = ±4 cm⁻¹. ^b vw = very weak, w = weak, m = medium, s = strong, vs = very strong, sh = shoulder.

of adsorption for these anionic species at Cu to overcome the electrostatic repulsion energy. Therefore, the Raman data support the conclusion drawn from the cyclic voltammetric results of very strong interaction of HDz⁻ with the Cu surface.

Even though these very negative potentials are more cathodic than the HDz⁻/H₃Dz⁻ reduction process, no major spectral features are observed that would suggest a change in the nature of the surface form. It appears that HDz⁻ remains the major surface species even after potentials at which HDz⁻ could be reduced. Upon recollection that a rotating disk electrode is used for acquisition of the surface spectra, an interpretation of these data is possible on the basis of the assumption that HDz⁻ is preferentially adsorbed over H₃Dz⁻ (as suggested by the cyclic voltammetric results). A steady-state population of HDz⁻ at the rotating surface could develop by reduction of the surface HDz⁻ to solution H₃Dz⁻ in an irreversible (i.e., slow) electron-transfer process, leaving a surface site available for rapid adsorption of another HDz⁻. Rotation of the electrode ensures that the *average* surface species is Raman detected. This average surface form would be HDz⁻ if the electron-transfer process is slow.

The absolute intensities of the surface signals at Cu are greater than those measured at Ag. However, these signals are the response of only monolayer, or submonolayer, quantities of HDz⁻, as evidenced by the current under the voltammetric wave shown in Figure 3b. It is documented that Cu does not exhibit surface-enhanced Raman scattering with 488.0-nm excitation.^{4,5} Thus, resonance enhancement appears to be the only mechanism contributing to the enhanced intensities measured in this system. Ag, on the other hand, is a SERS metal at 488.0 nm, and therefore, both enhancement mechanisms (SERS + RRS) contribute to the observed intensities for the HDz⁻/Ag system. The contribution of resonance enhancement per HDz⁻ is expected to be the same at Ag and Cu. The slightly greater intensity measured at Cu suggests a substantially greater surface population at Cu relative to Ag in pH 12 solutions at potentials cathodic of 0.0 V.

At potentials greater than 0.0 V, oxidation of HDz⁻ to the corresponding disulfide occurs. The surface spectra acquired at these potentials indicate the increasing presence of surface disulfide species. Several differences in the spectra mark this change. The first is that the band at 1158 cm⁻¹ becomes stronger in intensity than the band at 1215 cm⁻¹ as the surface population of disulfide relative to HDz⁻ increases. Second, the weak bands at ca. 724 and 1455 cm⁻¹ become distinctly visible. Third, the bands at ca. 1308 and 1508 cm⁻¹ become noticeably weaker. Lastly, the bands at ca. 1353 and 1398 cm⁻¹ increase in intensity at the expense of the bands at ca. 1340 and 1390 cm⁻¹.

While these spectral changes are similar to those observed at Ag, they are not identical. For example, at Ag, the band at ca. 1400 cm⁻¹ becomes clearly the strongest in the surface disulfide spectra. This is, in fact, the strongest band observed in the spectrum of an authentic disulfide sample presented in part 2.¹⁰ However, at Cu, the band at ca. 1355 cm⁻¹ is more prominent than the band at ca. 1400 cm⁻¹. The agreement between the surface disulfide spectra and the authentic disulfide spectrum at Cu is not as good as it is at Ag. The surface films visible at positive potentials on both electrodes are also different. At Ag, a deep reddish surface film, which is acetone soluble, is visible when the electrode is potentiostated at potentials greater than 0.2 V. However, the acetone-soluble film observed at Cu at 0.3 V is black and covers a layer of surface oxide, which becomes visible once the black layer is removed.

A possible explanation for these differences is that a combination of disulfide and HDz⁻ species exists at the Cu surface at these positive potentials. This effect could occur if a competition between formation/deposition of disulfide and oxidation of Cu to surface oxides occurs. These surface oxides are sparingly soluble in alkaline media and after dissolution would leave "bare" Cu patches to which HDz⁻ could adsorb before oxidation to the disulfide. In this way, a steady-state amount of surface disulfide, surface HDz⁻, and surface oxides would develop, and the surface spectra would represent this steady-state combination of surface species.

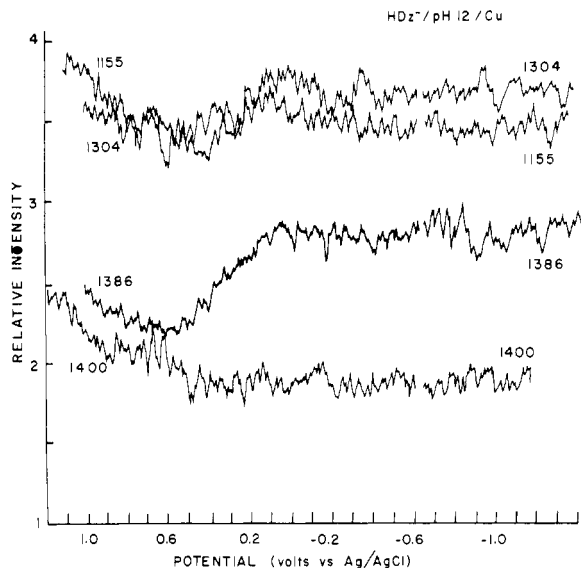


Figure 7. Surface Raman intensity vs. applied electrode potential for 1155-, 1304-, 1386-, and 1400- cm^{-1} surface bands for $\text{HDz}^-/\text{pH } 12$ solution/Cu.

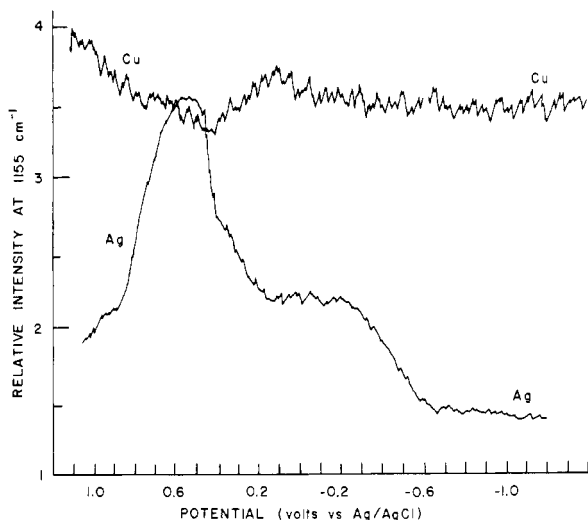


Figure 8. Comparison of surface Raman intensity vs. applied electrode potential for 1155- cm^{-1} surface band for $\text{HDz}^-/\text{pH } 12/\text{Ag}$ and $\text{HDz}^-/\text{pH } 12/\text{Cu}$.

The plots of Raman intensity vs. applied electrode potential are shown in Figure 7 for four of the surface Raman bands. These plots were obtained by monitoring the intensity of one band while the potential of the copper electrode at a rate of 10 mV/s is continuously changed. These data were acquired with a large spectrometer band-pass (ca. 10 cm^{-1}) to ensure that the effects of band maxima shifts on the observed intensity were minimal. The data for the potential region from -0.6 to $+1.0$ V were obtained on a single scan, starting at -0.6 V and proceeding to more positive potentials. The electrode surface was then repolished and immersed into the test solution, and the data in the region between -0.6 V and -1.2 V were obtained. The data were acquired in this manner to ensure that any chemically irreversible product of H_3Dz^- formed at these negative potentials that might be present on the surface did not interfere with the surface and redox behavior of HDz^- as potentials more anodic than the reduction potential of HDz^- are reached.

The data in these plots correlate well with the conclusions drawn from the single-potential Raman spectra discussed above. As suggested by the spectra in Figure 5, intensities in the potential region negative of 0.0 V do not change significantly as the electrode potential is altered. As the potential is made greater than 0.0 V, the surface intensity does diminish as the competition between

Table IV. Surface Raman Spectra of HDz^- Adsorbed Forms at Cu in pH 10 as a Function of Electrode Potential

frequency, cm^{-1} (rel intensity) ^b		-1.20 V	-1.00 V	-0.80 V	-0.60 V	-0.40 V	-0.20 V	0.00 V	0.20 V	0.40 V	0.60 V	0.80 V	open circuit
698 (w)	745 (s)	694 (w)	743 (s)	691 (vw)	743 (w)	694 (w)	747 (w)	696 (w)	747 (w)	694 (w)	749 (w)	743 (vw)	745 (m)
1003 (s)	1152 (vs)	1003 (s)	1155 (vs)	999 (m)	1003 (m)	1004 (m)	1152 (vs)	1000 (m)	1159 (vs)	1000 (m)	1157 (vs)	1155 (m)	1003 (m)
1216 (vs)	1305 (vs)	1218 (vs)	1307 (s)	1215 (vs)	1219 (vs)	1218 (vs)	1305 (vs)	1220 (vs)	1307 (s)	1159 (vs)	1220 (vs)	1213 (m)	1159 (s)
1347 (vs)	1423 (s)	1345 (vs)	1429 (m)	1349 (vs)	1349 (vs)	1344 (vs)	1422 (s)	1342 (s)	1422 (s)	1309 (s)	1342 (s)	1347 (m)	1216 (s)
	1464 (s)	1388 (m)	1463 (m)	1386 (s)	1386 (s)	1387 (s)	1466 (m)	1398 (vs)	1466 (m)	1344 (vs)	1403 (vs)	1347 (m)	1306 (s)
1510 (vs)	1595 (vs)	1423 (s)	1512 (vs)	1423 (m)	1461 (m)	1422 (sh)	1511 (m)	1422 (sh)	1457 (m)	1459 (m)	1424 (sh)	1463 (w)	1372 (s)
		1466 (s)	1594 (vs)	1463 (m)	1475 (m)	1466 (m)	1478 (m)	1478 (m)	1473 (m)	1478 (m)	1457 (m)	1501 (w)	1426 (m)
		1515 (vs)	1593 (vs)	1512 (vs)	1510 (m)	1478 (m)	1513 (s)	1513 (m)	1513 (m)	1508 (m)	1473 (m)	1583 (m)	1515 (m)
		1594 (vs)	1593 (vs)	1593 (vs)	1591 (s)	1591 (s)	1585 (m)	1583 (m)	1595 (s)				

^a Relative to the 488.0-nm argon ion laser excitation line. Measurement uncertainty (standard deviation) = $\pm 4 \text{ cm}^{-1}$. ^b vw = very weak, w = weak, m = medium, s = strong, vs = very strong, sh = shoulder.

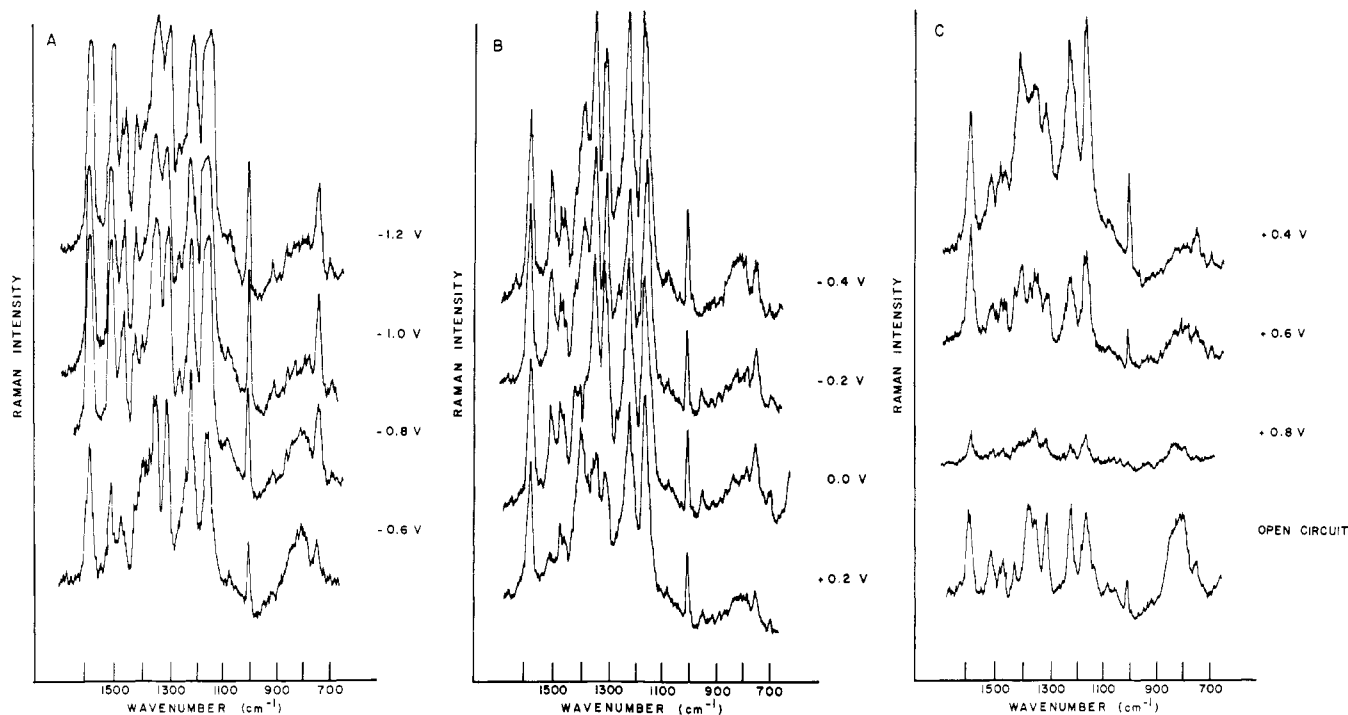


Figure 9. Surface Raman spectroelectrochemical data for 10^{-4} M HDz⁻/pH 10 solution at a Cu electrode: (A) $E_{app} = -1.2, -1.0, -0.8, -0.6$ V. (B) $E_{app} = -0.4, -0.2, 0.0, 0.2$ V. (C) $E_{app} = 0.4, 0.6, 0.8$ V, open circuit. Raman acquisition parameters are given in the text.

formation/deposition of disulfide and oxidation of the surface to sparingly soluble oxides occurs. Once the surface is oxidized to a less soluble form, however, multilayers of the disulfide are allowed to accumulate, and the intensities of the surface bands are observed to increase. This occurs at potentials greater than 0.6 V.

Figure 8 shows the Raman intensity for the 1155 cm^{-1} surface band vs. applied electrode potential for both Ag and Cu electrode surfaces. Differences between the absolute surface intensities measured are more readily seen. As discussed earlier, the intensities measured at Cu negative to 0.0 V are stronger and less variable than those measured at Ag in the same potential region. These data substantiate the conclusions drawn from the cyclic voltammetric and single-potential surface Raman data that the interaction of HDz⁻ with Cu is significantly greater than with Ag. Furthermore, they demonstrate the inability to control surface population of HDz⁻ at Cu relative to Ag at these potentials.

At potentials greater than 0.0 V, Figure 8 shows that the impact of oxidation of HDz⁻ to the disulfide is greater on the intensities measured at Ag than at Cu. The disulfide adsorbs readily in multilayers at the Ag surface before surface oxidation takes over at 0.6 V. At Cu, however, the surface processes occurring in this potential region are complex, and the decrease in the intensity in this region reflects this complexity as discussed above.

pH 10 Behavior. To demonstrate the effect of solubility of HDz⁻ on the adsorption at Cu, we performed a series of surface Raman experiments in pH 10 buffer solution in which the solubility of HDz⁻ is less than in pH 12 solution, owing to the dissociation constant of H₂Dz in aqueous, alkaline media. The surface Raman spectra acquired at selected potentials on a Cu electrode in a 10^{-4} M HDz⁻/pH 10 solution are shown in Figure 9 and the bands are tabulated in Table IV. The background spectra at Cu/pH 10 solution are featureless and resemble those presented in Figure 6 for the pH 12 solution. The extent of adsorption of HDz⁻ increases as its solubility is decreased, in accord with classical adsorption concepts. This behavior was demonstrated at a Ag electrode in part 2.¹⁰

Greater adsorption of a species dictates greater surface intensities measured for that species. Comparison of the spectra in Figures 9 and 5 reveals that the absolute intensities measured for the surface species in pH 10 solution are significantly greater than those measured in pH 12 solution, especially for the very negative

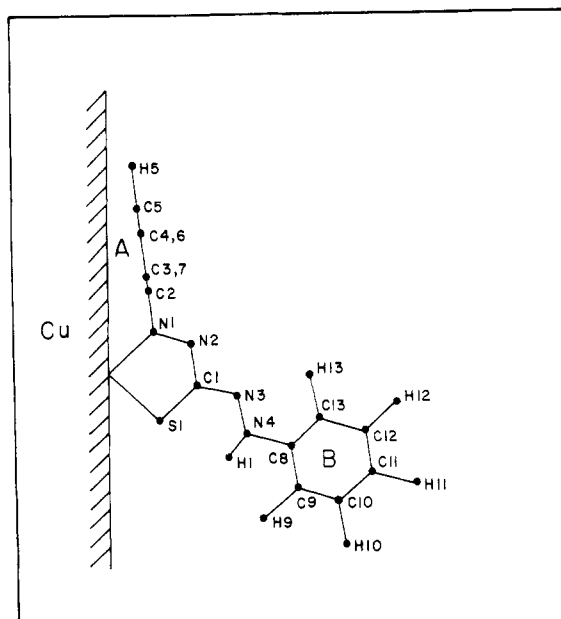


Figure 10. Orientation of adsorbed HDz⁻ at Cu electrode surface, drawn to scale. A and B denote the two phenyl groups.

potentials (e.g., -1.0 V, -1.2 V) in pH 10 solution. The attraction of the anionic HDz⁻ species for the negatively charged surface seems to be greater from pH 10 solution than from pH 12 solution.

The surface species existing in the different potential regions in pH 10 solution are presumed to be the same as those found at the surface in the pH 12 solution. Thus, at potentials negative of 0.0 V in pH 10 solution, the major surface species is assumed to be HDz⁻. At potentials positive of 0.0 V where oxidation to the disulfide occurs, the disulfide is expected to be the prominent surface species. The spectra shown in Figure 9 reflect the presence of these species, as was discussed above in the case of the pH 12 solution.

Orientation of Surface HDz⁻. On the basis of the similarity between the surface spectra and the Cu(HDz)₂ spectrum, the orientation of HDz⁻ at the Cu surface can be reasonably ap-

proximated to be that shown in Figure 10. This orientation is the same as that postulated for HDz⁻ at a Ag surface.^{10,11} This proposed orientation is based on the general bonding of HDz⁻ to the metal centers in metal dithizonates, which is essentially the same in all known cases. It is reasonable that the surface orientation for contact-adsorbed HDz⁻ at metal surfaces is similar. This orientation is not intended to represent the absolute orientation of HDz⁻ at the Cu surface. Such a detailed description of HDz⁻ adsorption cannot be drawn conclusively from the Raman spectroscopic data presented here. Rather, Figure 10 is intended to represent a reasonable orientation of contact-adsorbed HDz⁻ on the basis of the model of Cu(HDz)₂ used as a reference structure.

The assumed orientation shown in Figure 10 is drawn to scale by use of bond lengths and bond angles determined from X-ray crystallographic data on a representative metal dithizonate found in the literature. The crystal structure of Cu(HDz)₂ has not been reported, presumably due to the difficulty in obtaining single crystals of this complex. Therefore, X-ray crystal data from Ni(HDz)₂ were used.^{23,24} The differences between the crystal structures of metal dithizonates that have been reported are small, and therefore, the use of Ni(HDz)₂ X-ray data here is not expected to contribute significant error.

This orientation is drawn with the assumption that the S and N atoms are adsorbed at one Cu surface site, and that the molecule is perfectly planar and perpendicular to the Cu surface except for the azophenyl group (phenyl A), which is almost parallel to the Cu surface. The rotation of phenyl A to this position is postulated to occur as a mechanism to relieve the strain that would be incurred if it remained in the plane of the rest of the molecule. At the Cu surface, phenyl A is expected to be in its lowest energy (most stable) position as a result of π bonding with the metal surface. This orientation has been discussed in greater detail in a previous report for HDz⁻ at Ag.¹¹

Experimental Section

Spectroscopic and Electrochemical Equipment. The laser Raman system employed has been described in detail elsewhere.¹⁰ The 488.0-nm line of an Ar⁺ laser was used to excite all of the Raman spectra presented here. The Raman spectra were recorded at a band-pass of 5–6 cm⁻¹ with a scan rate of 1.0 cm⁻¹/s and a 2-s RC time constant unless otherwise specified. Laser power was typically 200 mW at the sample. The plots of Raman intensity vs. applied potential for the individual peaks were obtained by using a larger band-pass of ca. 10 cm⁻¹ to minimize the effects of band maxima shifts with changes in electrode potential on the observed intensity responses. Electrode potentials were controlled by use of a system of in-house design and construction consisting of a conventional three-electrode potentiostat²⁵ and a triangle wave generator.²⁶

The Raman spectroelectrochemical cell incorporated a rotating disk electrode and has been described in detail elsewhere.²² The primary purpose of rotation of the electrode surface in this study was to minimize the effects of photodecomposition of the surface species by the incident laser beam. In the work reported here, the electrode surface was positioned almost immediately adjacent to the front optical flat of the electrochemical cell such that a thin-layer configuration existed at the electrode surface. Hence, only a small amount of solution was sampled by the laser beam, and scattering from HDz⁻ in solution could not be observed.

The Cu-foil working electrode (99.99%) was polished with successively finer grades of alumina down to 0.05 μ m and rinsed with copious amounts of distilled, deaerated water. The resulting working electrode surface had a mirror finish. Prior to immersion in the HDz⁻ test solution for either cyclic voltammetric or Raman spectroscopic investigation, residual surface oxides were removed by precathodization in the background pH 12 or pH 10 buffer solution. This precathodization was carried out by potentiostating the working electrode at -1.0 V for ca. 30 s, moving the potential to -0.70 V, removing the electrode under potentiostatic control, and transferring it to the test solution in the appropriate cell. During the transfer step, care was taken to ensure that a drop of the supporting electrolyte solution remained covering the Cu surface such that reoxidation would be negligible.

The counterelectrode consisted of a Pt wire. All potentials were reported vs. a Ag/AgCl reference half-cell.

Materials and Reagents. Dithizone was purified as previously reported.¹⁰ The pH 10 and 12 aqueous alkaline buffer solutions were prepared and stored as described in an earlier report.¹⁰ Bis(1,5-diphenylformazan-3-yl) disulfide was synthesized after the manner of Kiwan and Irving.²⁷ 2,3-Diphenyl-2,3-dihydro-1,2,4-triazolium-5-thiolate was synthesized according to the procedure of Irving et al. involving oxidation of dithizone with ferricyanide.²⁸

Copper(II) dithizonate, Cu(HDz)₂ (IV), was prepared by dissolution of 0.97 g of Cu(NO₃)₂ in 100 mL of distilled water, and the pH was adjusted to the optimum value of 0.5 by the addition of dilute nitric acid. This was vigorously shaken with a solution of 0.9 g of purified dithizone in 200 mL of chloroform until the chloroform solution was completely violet and unchanging in color. The chloroform layer was separated, and the Cu(HDz)₂ was collected by evaporation of the solvent. The final product was obtained by recrystallization from chloroform.

All other materials were reagent grade or equivalent.

Acknowledgment. This work was supported by the National Science Foundation Grants CHE77-20491 and CHE77-14547. J.E.P. acknowledges support of this research in the form of a summer fellowship from the American Chemical Society Analytical Chemistry Division sponsored by FACSS.

Registry No. I, 46922-70-7; III, 25210-27-9; IV, 12213-13-7; 2,3-diphenyl-2,3-dihydro-1,2,4-triazolium-5-thiolate, 11065-31-9; Cu, 7440-50-8.

(23) Math, K. S.; Freiser, H. *Talanta* **1971**, *18*, 435.

(24) Mawby, A.; Irving, H. M. N. H. *J. Inorg. Nucl. Chem.* **1972**, *84*, 109.

(25) Mathis, D. E. Ph.D. Dissertation, University of North Carolina, Chapel Hill, NC, 1978.

(26) Woodward, W. S.; Rocklin, R. D.; Murray, R. W. *Chem. Biomed. Environ. Instrum.* **1979**, *9*, 95.

(27) Kiwan, A. M.; Irving, H. M. N. H. *J. Chem. Soc. B* **1971**, 901.

(28) Irving, H. M. H.; Kiwan, A. M.; Rupainwar, D. C.; Sahota, S. S. *Anal. Chim. Acta* **1971**, *56*, 205.